Received: 17 August 2023 | Accepted: 2 July 2024

DOI: 10.1111/1751-7915.14527

MICROBIAL BIOTECHNOLOGY
Open Access

RESEARCH ARTICLE

Design, construction and optimization of formaldehyde growth biosensors with broad application in biotechnology

Karin Schann[1] | **Jenny Bakker**[1] | **Maximilian Boinot**[1] | **Pauline Kuschel**[1] | **Hai He**[1,2] | **Maren Nattermann**[2] | **Nicole Paczia**[2] | **Tobias Erb**[2] | **Arren Bar-Even**[1,†] | **Sebastian Wenk**[1]

[1]Max Planck Institute of Molecular Plant Physiology, Potsdam-Golm, Germany

[2]Max Planck Institute for Terrestrial Microbiology, Marburg, Germany

Correspondence
Sebastian Wenk, Max Planck Institute of Molecular Plant Physiology, Am Mühlenberg 1, Potsdam-Golm 14476, Germany.
Email: wenk@mpimp-golm.mpg.de

Funding information
Bundesministerium für Bildung und Forschung, Grant/Award Number: 031B0850B (MetAFor)

Abstract

Formaldehyde is a key metabolite in natural and synthetic one-carbon metabolism. To facilitate the engineering of formaldehyde-producing enzymes, the development of sensitive, user-friendly, and cost-effective detection methods is required. In this study, we engineered *Escherichia coli* to serve as a cellular biosensor capable of detecting a broad range of formaldehyde concentrations. Using both natural and promiscuous formaldehyde assimilation enzymes, we designed three distinct *E. coli* growth biosensor strains that depend on formaldehyde for cell growth. These strains were engineered to be auxotrophic for one or several essential metabolites that could be produced through formaldehyde assimilation. The respective assimilating enzyme was expressed from the genome to compensate the auxotrophy in the presence of formaldehyde. We first predicted the formaldehyde dependency of the biosensors by flux balance analysis and then analysed it experimentally. Subsequent to strain engineering, we enhanced the formaldehyde sensitivity of two biosensors either through adaptive laboratory evolution or modifications at metabolic branch points. The final set of biosensors demonstrated the ability to detect formaldehyde concentrations ranging approximately from 30 μM to 13 mM. We demonstrated the application of the biosensors by assaying the in vivo activity of different methanol dehydrogenases in the most sensitive strain. The fully genomic nature of the biosensors allows them to be deployed as "plug-and-play" devices for high-throughput screenings of extensive enzyme libraries. The formaldehyde growth biosensors developed in this study hold significant promise for advancing the field of enzyme engineering, thereby supporting the establishment of a sustainable one-carbon bioeconomy.

Karin Schann, Jenny Bakker and Maximilian Boinot contributed equally to this study.

[†]Deceased.

INTRODUCTION

Formaldehyde is an important metabolite in methylotrophic one-carbon (C_1) metabolism. Methylotrophs growing on methanol assimilate formaldehyde into biomass via the ribulose monophosphate (RuMP) cycle, the xylulose monophosphate (XuMP) cycle or the serine cycle (Antoniewicz, 2019; Zhang et al., 2017). Since methanol can be produced electrochemically from CO_2 (Bowker, 2019), it is expected to become an important feedstock for a sustainable, CO_2-based bioeconomy that uses native or synthetic methylotrophs to produce value-added products (Claassens et al., 2019; García & Galán, 2022; Whitaker et al., 2015).

As the engineering of natural methylotrophs for bioproduction can be challenging (Schada Von Borzyskowski et al., 2015), recent efforts have focused on engineering biotechnological hosts like *Saccharomyces cerevisiae*, *Escherichia coli* and *Cupriavidus necator* to grow on methanol (synthetic methylotrophy) (Chen et al., 2020; Claassens et al., 2020; Espinosa et al., 2020; He et al., 2020; Keller et al., 2022; Kim et al., 2020). However, the lack of efficient methanol dehydrogenases (MDHs) that can be heterologously expressed in common microbial hosts presents a major bottleneck for engineering efficient growth on methanol. The widely used NAD-dependent MDHs can be easily expressed but display poor activities, including low catalytic rates and high K_M values. On the other hand, PQQ-dependent MDHs are very efficient but are difficult to express (Krüsemann et al., 2023; Le et al., 2021). Thus, engineering efficient MDHs for synthetic methanol assimilation is an open challenge to establish a methanol-based bioeconomy.

Formate is another attractive C_1 feedstock. Like methanol, it can be efficiently produced from CO_2 and could serve as a sustainable growth substrate for microbes (Yishai et al., 2016). A synthetic enzyme cascade that reduces formate to formaldehyde has been proposed (Bar-Even, 2016). This route would vastly increase the number of formate assimilation pathways as it could be combined with both natural and synthetic formaldehyde assimilation pathways (e.g. the homoserine cycle or the formolase pathway (He et al., 2020; Siegel et al., 2015)). While recent studies were able to show the activity of the enzyme cascade (Hu et al., 2022; Wang et al., 2021) (Nattermann et al., 2023), none of them was able to achieve bacterial growth via these routes. Hence, enzyme engineering and optimization for efficient formate to formaldehyde reduction is still required.

To establish or optimize formaldehyde dependent growth, it is necessary to screen for formaldehyde producing enzymes and assess their in vivo activity. Here, cell-based biosensors could be a valuable tool to detect intracellular formaldehyde production. Cell-based biosensors have become attractive and cost-effective tools in biotechnological applications ranging from environmental monitoring to clinical diagnosis (Gupta et al., 2019). Compared to chemical sensors, they are self-assembling, easy to handle and of low environmental impact. An ideal biosensor should be highly specific and detect a wide range of concentrations of the target molecule. Furthermore, it should have a high signal-to-noise ratio and a low false-positive rate (Dietrich et al., 2010). The concept of growth-coupled design has been recognized as a powerful methodology for the generation of cell-based biosensors that can detect key metabolites or enzyme activities with said characteristics (Aslan et al., 2020; Wenk et al., 2020).

While many electrochemical formaldehyde biosensors based on immobilized enzymes have been developed (Herschkovitz et al., 2000; Ling & Heng, 2010; Marzuki et al., 2012), they cannot assess intracellular formaldehyde production. Also, the widely used NASH assay (Nash, 1953) only allows indirect assessment of intracellular formaldehyde production. Opposed to this, cellular biosensors that produce a measurable signal upon formaldehyde detection could allow direct assessment of intracellular formaldehyde production. One such formaldehyde biosensor has been developed by Woolston et al. The plasmid-based *E.coli* biosensor produces a fluorescent or luminescent signal in the presence of formaldehyde and has a detection range of 1–250 μM (Woolston et al., 2018). An alternative approach for constructing cellular biosensors could involve linking formaldehyde production to cellular growth (growth biosensors). As demonstrated in previous studies, strategic gene deletions could be implemented to create auxotrophies that would only be relieved when the molecule of interest (in this case formaldehyde) is present inside the cell (Aslan et al., 2020; Orsi et al., 2021; Wenk et al., 2020). Using these biosensors, would enable screening of large libraries for enzyme candidates that produce formaldehyde without the need for sophisticated laboratory equipment. Furthermore, due to their robustness and the simple readout, they could be used for long-term evolution experiments.

In this study, we designed and engineered three formaldehyde growth biosensors that can detect a broad range of formaldehyde concentrations. First, we screened the metabolic landscape of *E. coli* for suitable formaldehyde entry points (natural and synthetic) and determined three suitable formaldehyde assimilation reactions for the biosensor design. Based on these reactions, we designed three growth biosensors in which formaldehyde serves as a precursor for different essential metabolites (Figure 1). Using flux balance analysis (FBA), we estimated the formaldehyde dependency of the different strains (Figure S1). Then, we engineered, validated and optimized the biosensor strains. In detailed characterization experiments, we determined the formaldehyde sensitivity of each biosensor and could

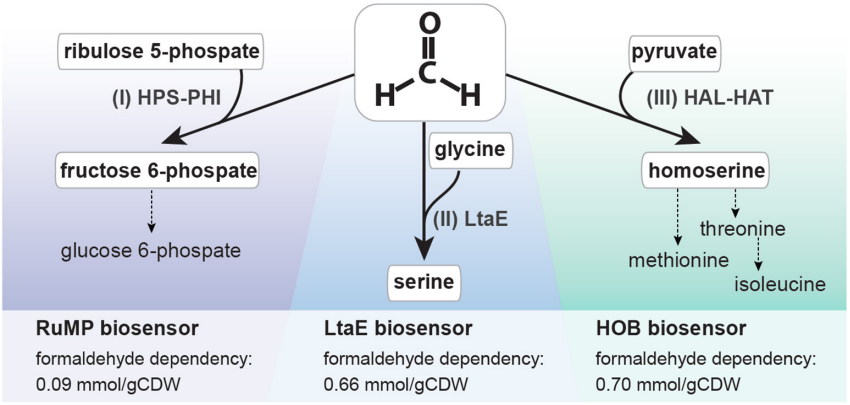

FIGURE 1 Formaldehyde detection via three different *E. coli* growth biosensors. Formaldehyde (circled in green) is an important metabolite and a widely used commodity chemical. For its detection, three *E. coli* biosensors depending on formaldehyde assimilation for cell growth were designed. Each strain is based on a different set of assimilating enzymes. (I) The RuMP biosensor is based on the RuMP cycle enzymes 3-hexulose-6-phosphate synthase (HPS) and 6-phospho-3-hexuloisomerase (PHI) to convert formaldehyde and ribulose 5-phosphate (Ru5P) into the essential metabolites fructose-6-phosphate (F6P) and glucose 6-phosphate (G6P). (II) The LtaE biosensor utilizes the promiscuous serine aldolase activity of low-specificity L-threonine aldolase (LtaE) to condense formaldehyde and glycine into the essential amino acid serine. (III) The HOB biosensor is based on the promiscuous 4-hydroxy-2-oxobutanoate (HOB) aldolase (HAL) reaction of the *E. coli* enzyme 2-keto-3-deoxy-L-rhamnonate aldolase (encoded by *rhmA*) followed by a HOB transaminase (HAT) reaction which assimilate formaldehyde and pyruvate into homoserine. Homoserine is the precursor of the essential amino acids threonine, isoleucine and methionine. The formaldehyde dependency of each strain (mmol/gCDW) was calculated by flux balance analysis based on the *E. coli* genome-scale metabolic model and is indicated in the bottom of the figure.

show that they span a combined detection range from ~30 μM to ~13 mM. We also provide insights into potential applications of the biosensors. Thereafter, we provided insights into potential applications of the biosensors, by testing several widely used MDHs in the HOB biosensor. We benchmarked their in vivo activities and demonstrated that the biosensors could be highly useful for enzyme discovery or engineering.

EXPERIMENTAL PROCEDURES

Chemicals and reagents

Primers were synthesized at Integrated DNA Technologies (IDT). DNA fragments were amplified with the high-fidelity polymerase PrimeSTAR Max DNA Polymerase from TaKaRa and colony PCR reactions were performed using DreamTaq polymerase (Thermo Fisher Scientific). FastDigest restriction enzymes and T4 DNA ligase from Thermo Fisher Scientific were used for restriction-based cloning. The kits used for plasmid isolation and PCR cleanup were purchased from Thermo Fischer Scientific. All chemicals used in the plate reader experiments were ordered from Sigma-Aldrich.

Growth media

For cloning and strain engineering, cultures were grown in lysogeny broth (LB) medium (10 g/L NaCl, 10 g/L Tryptone, 5 g/L Yeast Extract) supplemented with the relevant antibiotic (50 μg/mL kanamycin, 30 μg/mL chloramphenicol or 100 μg/mL streptomycin). Diaminopimelate (DAP, 0.25 mM) needs to be supplemented to the growth media of the HOB strain due to the *asd* knockout. During growth experiments, cells were cultivated in M9 minimal medium (50 mM Na_2HPO_4, 20 mM KH_2PO_4, 1 mM NaCl, 20 mM NH_4Cl, 2 mM $MgSO_4$ and 100 μM $CaCl_2$), supplemented with trace elements (134 μM EDTA, 31 μM $FeCl_3$, 6.2 μM $ZnCl_2$, 0.76 μM $CuCl_2$, 0.42 μM $CoCl_2$, 1.62 μM H_3BO_3, 0.081 μM $MnCl_2$) and the relevant carbon sources.

Strains

Plasmid construction was done in *E. coli* DH5α. The *E. coli* SIJ488 strain, which is derived from K-12 MG1655, was used as a base strain for the biosensor strains (Jensen et al., 2015). The KEIO collection was used as donor strains to prepare the P1 donor lysates for phage transduction (Baba et al., 2006). Strains used in this study are listed in Table S1 and plasmids in Table S2.

Strain engineering

The biosensor strains were constructed by using recombineering techniques to modify the SIJ488 base strain. Deletions were made by P1 phage transduction and λ-Red recombineering as detailed in (Wenk et al., 2018). To make deletions with λ-Red recombineering, a kanamycin or chloramphenicol antibiotic cassette, flanked by FRT sites, was amplified with primers containing

50 bp homology arms that are flanking the region of the target gene. This linear DNA fragment was introduced in the cell by electroporation after 1 h of inducing the λ-Red recombineering machinery with 15 mM arabinose. The cell suspension was then plated on LB plates containing the relevant antibiotics and a colony PCR was performed to confirm successful gene deletions. The antibiotics cassettes were removed by inducing the flippase with 50 μM L-rhamnose for at least 4 h and removal was confirmed by a colony PCR. For P1 phage transduction, the KEIO collection strain with the desired knockout was grown in LB supplemented with 5 mM $CaCl_2$ until an OD ~0.3. Then the culture was infected with P1vir (Ikeda & Tomizawa, 1965) stock lysate for 2–4 h. The cells were pelleted by centrifugation and the supernatant was filtered through a 0.22-μm filter to obtain the donor lysate that was then used for the transduction. The deletion in the relevant strain was made by resuspending the pellet of an overnight culture in P1 salts (LB supplemented with 10 mM $CaCl_2$ and 5 mM $MgSO_4$). P1 donor lysate was added to this cell suspension and incubated for 30 min at 30°C. After recovery for 1 h in LB with ~100 mM sodium citrate, the cells were placed on selective plates containing 5 mM sodium citrate and kanamycin. The antibiotics cassette was later removed by inducing the flippase. Knockouts and removal of the antibiotic cassette were confirmed by a colony PCR.

Genomic integrations were made via a conjugation-based genetic recombination method as detailed in (Wenk et al., 2018). In short, the synthetic operon was cloned into a vector which contains the chloramphenicol resistance gene (*cam*^{R}) and 600 bp homology arms that are compatible with the genomic integration site. Furthermore, the vector contains a levansucrase gene (*sacB*) and the *traJI* gene to allow for the transfer of the plasmid. After transformation in chemically competent ST18, the colonies growing on chloramphenicol plates were screened by a colony PCR. A positive clone was then used for the conjugation. After conjugation, the SIJ488 strains growing on chloramphenicol plates were screened by sucrose counter selection and kanamycin resistance tests to isolate recombinant SIJ488 strains with the correctly integrated synthetic operon. The antibiotics cassette was removed by inducing the flippase. The genomic integration and antibiotics cassette removal were confirmed by a colony PCR.

Synthetic-operon construction

All genes (see Appendix S1) were codon optimized for *E. coli* K-12, after which a 6xHis-tag was added to the N-terminal side. Subsequently, the genes were inserted into a cloning vector, which attaches a synthetic ribosomal binding site upstream of the gene (Zelcbuch et al., 2013). These cloning vectors were used to assemble synthetic operons via restriction and ligation using the protocol as described in (Wenk et al., 2018).

The assembled construct was then transferred to the pZ expression vector which contains the p15A ori, a streptomycin resistance gene, and attaches the P_{pgi}-20 promoter to the gene/operon of interest. This assembly was performed using the restriction enzymes EcoRI and PstI. (Wenk et al., 2018).

Growth experiments

Prior to all growth experiments, the strains (see Table S1) were streaked out from the glycerol stock on LB plates (supplemented with the respective antibiotic and 0.25 mM DAP in the case of the HOB biosensor) and grown overnight at 37°C. From these plates, precultures in relaxing liquid M9 medium (as indicated in Table S3) were inoculated for overnight growth at 37°C and 220 rpm. The cells were harvested (11,000 g, 1 min), washed three times with M9 minimal medium, and diluted to a final OD_{600} of 0.01 in the desired medium. In a Nunc 96-well microplates (Thermo Fisher Scientific), 150 μL of the culture was added to each well and the wells were covered with 50 μL of mineral oil (Sigma-Aldrich) to prevent evaporation. The growth experiments were performed in the BioTek Epoch2 plate reader (BioTek Instrument, USA) which measured the optical density after each kinetic cycle. A cycle consists of 12 shaking steps in which 60 s of linear and 60 s of orbital shaking were alternated (1 mm amplitude). The OD_{600} was corrected to present the $OD_{600\_cuvette}$ by dividing the OD_{600_plate} by the correction factor of 0.23. The mean of the technical duplicates is shown in the growth curves. The sensitivity plots show the average values of three independent experiments and their respective standard deviation. Data was only included when all three experiments showed growth.

Adaptive laboratory evolution of the LtaE biosensor

The experiment was conducted with the rbsA LtaE biosensor strain expressing *Cg*MDH from a plasmid. Four 14 mL glass tubes with biological replicates were cultivated in a selective medium (M9 minimal medium with 10 mM glucose, 10 mM glycine, 50 μM $MnCl_2$ and 500–10 mM methanol) for 15 weeks during which the methanol concentration was stepwise reduced. Whenever the strain reached an $OD_{600} > 0.5$ the culture was diluted into fresh medium to an OD_{600} of 0.01. First, the strains were cultivated for one generation with 500 mM methanol. Then the methanol concentration was reduced to 100 mM for another generation. Thereafter, the culture was diluted into a medium containing 50 mM methanol. After 10 days, the methanol concentration was

reduced to 25 mM. In the following, the methanol concentration was reduced to 20 mM, 15 mM and finally to 10 mM changing the methanol concentration approximately every 10 days. Growth in a selective medium with 10 mM methanol was continued for 4 weeks. Then, single colonies were isolated from the growing populations and analysed via growth experiments and whole genome sequencing.

Whole-genome sequencing

Genomic DNA was extracted using a commercial kit (Mackerey Nagel) starting from 2 to 4 mL of overnight culture in LB. A minimum of 300 ng was sent for sequencing to NovoGene. Results were analysed using the open source breseq software (Barrick et al., 2014). All NGS data was deposited at the Genome Sequence Archive.

In vitro characterization of LtaE and LtaE*

Kinetics for LtaE and LtaE* were determined by HPLC–MS detection of serine. Reaction mixtures contained 100 mM $KxHyPO_4$, 5 mM $MgCl_2$, 100 μM pyridoxal phosphate, 1 μM enzyme and the glycine and formaldehyde concentrations provided in Figure S3. After incubation at 30°C (timepoints 0.5, 1, 2, and 3 min), samples were quenched in formic acid to a final concentration of 5%. A serine standard in the reaction matrix was run alongside the samples. Serine was detected via HPLC–MS and quantified against the standard. The initial slope of serine production was calculated by linear fit in GraphPad Prism v9 and Michaelis Menten kinetics were constructed in the same program using standard setting.

HPLC–MS detection of amino acids

Quantitative determination of serine and glycine was performed using a LC–MS/MS. The chromatographic separation was performed on an Agilent Infinity II 1290 HPLC system using a ZicHILIC SeQuant column (150 × 2.1 mm, 3.5 μm particle size, 100 Å pore size) connected to a ZicHILIC guard column (20 × 2.1 mm, 5 μm particle size) (Merck KgAA) a constant flow rate of 0.3 mL/min with mobile phase A being 0.1% formic acid in 99:1 water: acetonitrile (Honeywell, Morristown, New Jersey, USA) and phase B being 0.1% formic acid 99:1 acetonitrile: water (Honeywell, Morristown, New Jersey, USA) at 25°C.

The injection volume was 1 μL. The mobile phase profile consisted of the following steps and linear gradients: 0–5 min from 80% to 65% B; 5–7 min from 65% to 20% B; 7–9 min constant at 20% B; 9–10 min from 20% to 80% B; 10–12 min constant at 80% B. An Agilent 6495 ion funnel mass spectrometer was used in positive mode with an electrospray ionization source and the following conditions: ESI spray voltage 2000 V, nozzle voltage 1000 V, sheath gas 250°C at 12 L/min, nebulizer pressure 60 psig and drying gas 100°C at 11 L/min. Compounds were identified based on their mass transition and retention time compared to standards. Chromatograms were integrated using MassHunter software (Agilent, Santa Clara, CA, USA). Absolute concentrations were calculated based on an external calibration curve prepared in the sample matrix.

Mass transitions, collision energies, Cell accelerator voltages, and Dwell times have been optimized using chemically pure standards. The parameter settings of all targets are given in Table S4.

Flux balance analysis

Flux balance analysis (FBA) was used for calculating formaldehyde dependency of the biosensor strains. The modelling was conducted with COBRApy (Ebrahim et al., 2013) using the most updated *E. coli* genome-scale metabolic model *i*ML1515 (Monk et al., 2017) with curations and changes. The lowest possible fluxes of formaldehyde uptake in the biosensor strains for different growth rates were calculated. Formaldehyde dependency of the biosensors was estimated from the slope of growth rates and minimal formaldehyde uptake rates from the modelling. The full code, including the construction of models for selection strains, was deposited at Zenodo.

Code availability

MATLAB and breseq codes used for the analysis of the experiments are available from the corresponding author upon request. The flux balance analysis code is available openly on Zenodo (https://zenodo.org/record/8009619).

RESULTS

Strain construction and characterization

In the following, we describe the design, construction and characterization of the three different formaldehyde biosensors created in this study:

(i) The RuMP biosensor is based on the natural activity of the RuMP cycle enzymes 3-hexulose-6-phosphate synthase (HPS) and 6-phospho-3-hexuloisomerase (PHI) to detect formaldehyde. Formaldehyde is condensed with ribulose

5-phosphate (Ru5P) and is subsequently assimilated into the essential metabolites fructose 6-phosphate (F6P) and glucose 6-phosphate (G6P).

(ii) The LtaE biosensor is based on the promiscuous activity of the enzyme low-specificity L-threonine aldolase (LtaE) to detect formaldehyde. Formaldehyde is condensed with glycine to form the essential metabolite serine.

(iii) The HOB biosensor is based on the promiscuous 4-hydroxy-2-oxobutanoate (HOB) aldolase (HAL) activity of the enzyme 2-keto-3-deoxy-L-rhamnonate aldolase (RhmA) followed by a HOB transaminase (HAT) reaction to detect formaldehyde. Formaldehyde is condensed with pyruvate and serves as a precursor for the essential metabolites: methionine, threonine and isoleucine.

As the biosensor strains rely on formaldehyde to grow, we conducted flux balance to assess their growth dependency on formaldehyde (see Figure 1 and Figure S1 and Experimental Procedures). Then, we engineered the designed strains by implementing gene deletions that create the required auxotrophies. Thereafter, the gene(s) encoding the respective formaldehyde assimilation enzyme were expressed from a defined genomic locus. The sensor strains were then analysed experimentally to determine their formaldehyde sensitivity.

As formaldehyde is highly toxic at very low concentrations (<500 μM in *E. coli* (Nattermann et al., 2023)), the non-cytotoxic substrate sarcosine (N-methylglycine) was used to enzymatically produce formaldehyde in situ. For this, we used the enzyme sarcosine oxidase (SoxA) which efficiently and irreversibly oxidizes sarcosine to formaldehyde and glycine (K_M of 3.6 mM and k_{cat} of 14 s^{-1} (Nishiya et al., 2016)). We chose this approach as it produced highly reproducible results and was used in previous studies for the same purpose (He et al., 2018, 2020). For all characterization experiments, the formaldehyde biosensors were transformed with the same plasmid expressing *soxA* under the control of a constitutive promoter. We also validated the results obtained with sarcosine by directly adding formaldehyde to the culture medium which resulted in highly similar formaldehyde sensitivities (Figure S2).

By controlling the cultivation conditions with saturated amounts of all required carbon sources and supplements except the formaldehyde source, we obtained highly reliable growth phenotypes for all the biosensors where the final OD_{600} correlated with the amount of added formaldehyde precursor. We define the formaldehyde sensitivity of the biosensors as follows:

The formaldehyde sensitivity of a biosensor is defined by the lowest concentration of formaldehyde at which the strain shows a measurable growth signal (max. $OD_{600} > 0.1$) within the experimental time frame (<200 h). The sensitivity inversely correlates with the concentration of detectable formaldehyde, i.e. the lower the formaldehyde concentration that can be detected by the strain, the higher its formaldehyde sensitivity. We note that in the case of two strains growing at the same concentration of formaldehyde, the strain that grows earlier and/or to a higher OD_{600} is considered more sensitive.

Construction and characterization of the RuMP biosensor

Based on the natural formaldehyde assimilating enzymes of the RuMP cycle (HPS and PHI), we designed the RuMP biosensor with an estimated formaldehyde dependency of 0.09 mmol/gCDW (as estimated by FBA) (Figure 2A). Through the deletions indicated in Figure 2A, the strain becomes auxotrophic for fructose 6-phosphate (F6P) and glucose 6-phosphate (G6P) when cultivated on a carbon source from lower metabolism (e.g., succinate). These auxotrophies could be relieved if formaldehyde is condensed with ribulose 5-phosphate (Ru5P) (derived from xylose provided in the medium) and assimilated into F6P via HPS and PHI.

Deletion of all the required genes resulted in the RuMP parent strain ($RuMP_{Parent}$). Then, the HPS and PHI genes were cloned into a synthetic operon either with a medium or a strong ribosome binding site (rbs) (rbsC and rbsA, respectively) (Zelcbuch et al., 2013). The operons were expressed from the genome of $RuMP_{Parent}$ under the control of a strong constitutive promoter creating the two RuMP sensor strains $RuMP_C$ and $RuMP_A$ (Table S1). To confirm the ability of $RuMP_A$ and $RuMP_C$ to detect intracellularly produced formaldehyde, we transformed the strains with a plasmid encoding SoxA. We cultivated the resulting strains with a defined concentration of sarcosine to compare their formaldehyde sensitivity. As $RuMP_A$ showed a higher formaldehyde sensitivity compared to $RuMP_C$ (Figure 2B), we used $RuMP_A$ for more detailed characterization. Testing $RuMP_A$ with a sarcosine gradient revealed an estimated formaldehyde detection range between 1 and 13 mM (Figure 2C). Sarcosine concentrations below 1 mM resulted in an unreliable growth phenotype (data not shown) and were thus excluded from the biosensors formaldehyde detection range.

Construction and characterization of the LtaE biosensor

The design of the LtaE biosensor is based on the promiscuous serine aldolase activity of the *E. coli* enzyme

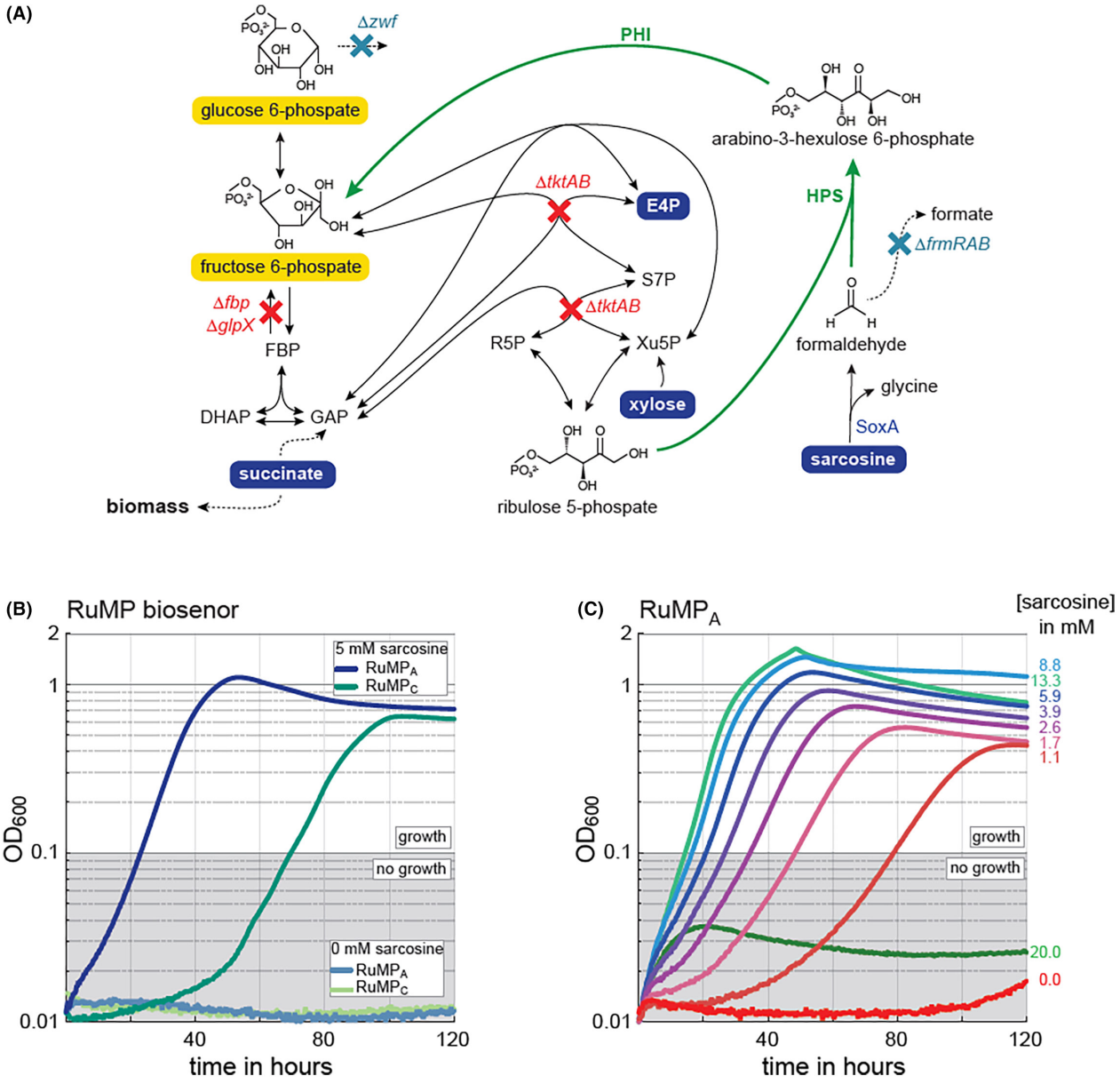

FIGURE 2 The RuMP biosensor detects formaldehyde in the millimolar range. (A) Metabolic scheme of the RuMP biosensor. The strain uses the RuMP cycle enzymes HPS and PHI for the assimilation of formaldehyde and ribulose 5-phosphate into fructose 6-phosphate (F6P) which is further converted to glucose 6-phosphate (G6P). Deletions of native enzymes generating F6P and G6P as well as of enzymes draining the intermediates were performed to generate the auxotrophy. *hps* and *phi* from *Bacillus methanolicus* were expressed from the genome with either expression regulated by a medium (rbsC) or strong ribosome binding site (rbsA). Additionally, SoxA was expressed from a plasmid to allow sarcosine conversion into formaldehyde as a stand-in for extracellular formaldehyde supplementation. (B) The RuMP biosensors with rbsC ($RuMP_C$) or rbsA ($RuMP_A$) were cultivated in minimal containing all relevant carbon sources with and without the addition of 5 mM sarcosine. Only when sarcosine was added to the medium, the strains grew, indicating their dependency on formaldehyde. (C) To characterize the RuMP biosensor in more detail, the $RuMP_A$ strain was cultivated with a sarcosine gradient ranging from 0 to 20 mM. The gradient revealed a correlation of growth and sarcosine concentration between 1.1 and 13.3 mM. DHAP, dihydroxyacetone phosphate; E4P, erythrose 4-phosphate; FBP, fructose 1,6-bisphosphate; GAP, glyceraldehyde 3-phosphate; R5P, ribose 5-phosphate; S7P, sedoheptulose 7-phosphate; X5P, xylulose 5-phosphate; *fbp*, fructose 1,6-bisphosphatase 1; *glpX*, fructose 1,6-bisphosphatase 2; *tktAB*, transketolase 1 and 2; *frmRAB*, formaldehyde detoxification system; *zwf*, glucose 6-phosphate dehydrogenase; SoxA, sarcosine oxidase; HPS, 3-hexulose-6-phosphate synthase; PHI, 6-phospho-3-hexuloisomerase. Figure elements: Yellow background: Auxotrophy; blue circle: Substrate; red cross: Deletion causing auxotrophy; cyan cross: Non-essential deletion; green arrow: Formaldehyde assimilation flux; dashed arrow: Multi enzymatic reaction.

LtaE (Contestabile et al., 2001). The enzyme was previously shown to condense formaldehyde and glycine to serine in vivo (He et al., 2020). Expressing *ltaE* in a serine auxotrophic strain that cannot synthesize serine from 3-phosphoglycerate (Δ*serA*) or from glycine and methylene-THF (Δ*glyA*) should create a formaldehyde biosensor, that is only capable of growing on glucose and glycine when formaldehyde is present inside the

cell (Figure 3A). Using FBA, we estimated that the LtaE biosensor has a formaldehyde dependency of 0.66 mmol/gCDW.

By deleting the genes indicated in Figure 3A as well as the endogenous *ltaE* gene, we created the $LtaE_{parent}$ strain. Next, we integrated *ltaE* with either rbsC or rbsA into the genome and expressed it under the control of a strong constitutive promoter (Figure 3A). The resulting strains, $LtaE_C$ and $LtaE_A$, were transformed with the SoxA plasmid and tested for their ability to detect

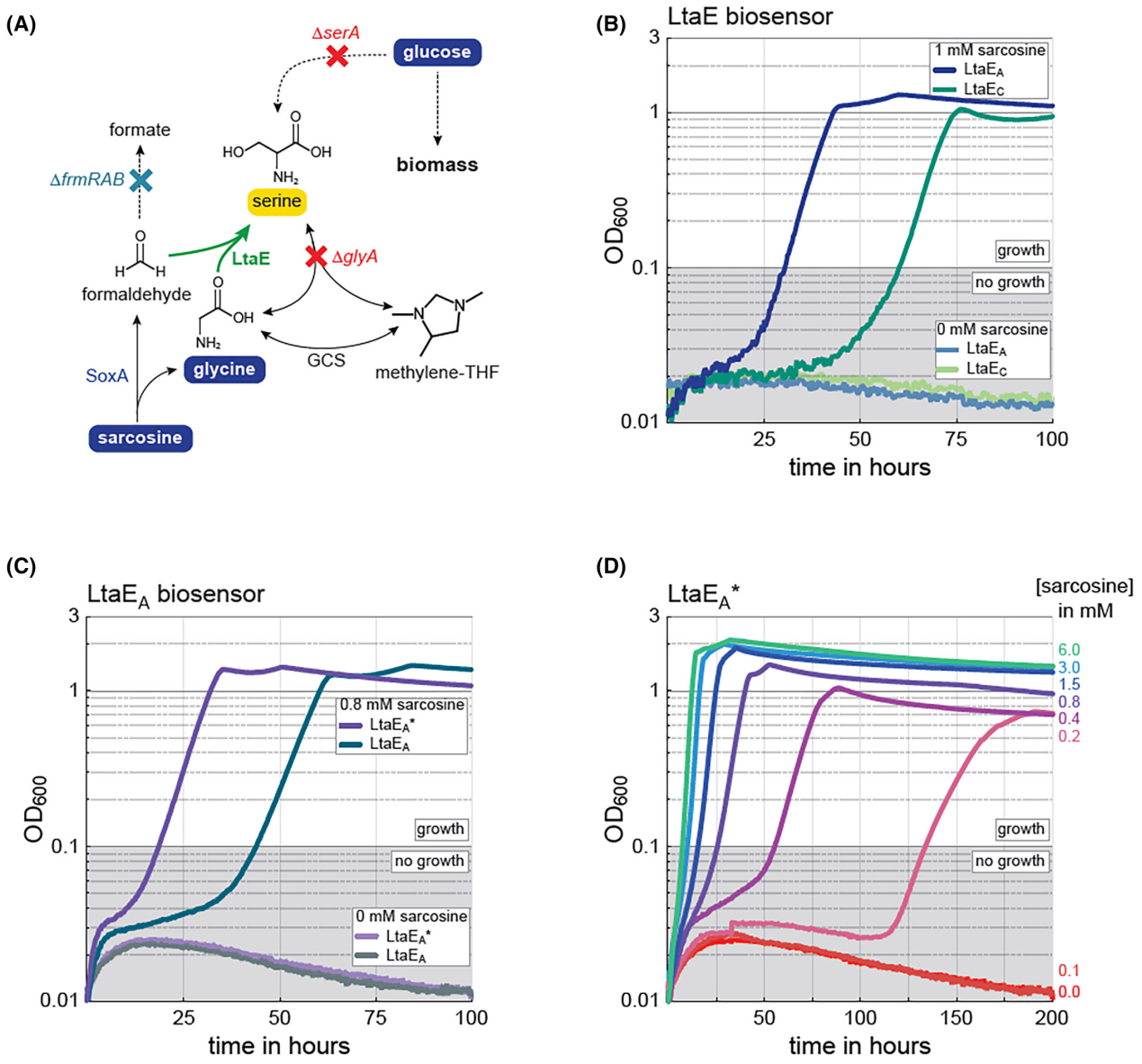

FIGURE 3 The LtaE biosensor detects formaldehyde in the milli- to micromolar range. (A) Metabolic scheme of the LtaE biosensor. The strain is based on the promiscuous activity of the LtaE enzyme that condenses formaldehyde and glycine into serine. Therefore, a serine auxotrophy was established by deleting essential genes for serine biosynthesis. To assimilate formaldehyde and glycine into serine, *ltaE* was expressed from the genome either with a medium or strong ribosome binding site (rbsC or rbsA, respectively). To generate intracellular formaldehyde from sarcosine, SoxA was expressed from a plasmid. (B) The LtaE biosensors with either rbsC or rbsA ($LtaE_C$ and $LtaE_A$) were cultivated in a minimal medium containing all relevant carbon sources with and without the addition of 1 mM sarcosine. The strains only grew in the presence of sarcosine, indicating their dependency on formaldehyde. (C) An amino acid exchange (LtaE_C188Y) observed in an ALE experiment was introduced into the $LtaE_A$ biosensor, creating the $LtaE^*_A$ biosensor. A comparison of the $LtaE_A$ and the $LtaE^*_A$ biosensor showed that the $LtaE^*_A$ showed a 2-fold faster growth when cultivated with 0.8 mM sarcosine. (D) For detailed characterization of the formaldehyde sensitivity, the $LtaE^*_A$ biosensor was cultivated in a gradient of sarcosine concentrations ranging from 0 to 6 mM. The gradient revealed a correlation between growth and sarcosine concentration between 0.2 and 6 mM. *GlyA*, serine hydroxymethyl transferase; *serA*, phosphoglycerate dehydrogenase; *frmRAB*, formaldehyde detoxification system; SoxA, sarcosine oxidase; LtaE, threonine aldolase; GCV, glycine cleavage system. Figure elements: Yellow background: Auxotrophy; blue circle: Substrate; red cross: Deletion causing auxotrophy; cyan cross: Non-essential deletion; green arrow: Formaldehyde assimilation flux; dashed arrow: Multi enzymatic reaction.

intracellularly produced formaldehyde. As the $LtaE_A$ strain showed a higher formaldehyde sensitivity compared to the $LtaE_C$ (Figure 3B), all subsequent experiments were carried out with the more sensitive $LtaE_A$.

The LtaE biosensor is the only strain that depends on the activity of one enzyme to relieve its auxotrophy. Thus, we hypothesized that the strain could be "easily" evolved for better LtaE activity. To test this, $LtaE_A$ was transformed with an MDH from *Corynebacterium glutamicum* (*Cg*MDH) and continuously cultivated in closed tubes with decreasing concentrations of methanol. In this experiment, we used methanol instead of sarcosine as a formaldehyde source as the low turnover of MDH presumably yields lower intracellular formaldehyde levels, which could favour LtaE evolution towards a lower K_M. The short-term evolution experiment resulted in strains with improved methanol dependency. When analysing these strains via whole genome sequencing, we identified a point mutation in the *ltaE* gene that lead to a dedicated amino acid exchange (C188Y). Although, the respective amino acid is not located near the active site of the enzyme, detailed in vitro characterization revealed a lowering of the K_M for glycine, yielding a two-fold improvement in k_{cat}/K_M of LtaE (C188Y) compared to LtaE (WT) (Figure S3).

As the $LtaE_A$ biosensor carrying the C188Y mutation (from here on termed $LtaE_A$*) showed a consistently higher formaldehyde sensitivity than the original $LtaE_A$ biosensor (Figure 3C), we went on to characterize this strain in more detail. To this end, we conducted a growth experiment with a sarcosine gradient, which revealed an estimated formaldehyde detection range of the $LtaE^*_A$ biosensor between 0.2 and 6 mM (Figure 3D).

Construction and characterization of the HOB biosensor

The HOB biosensor is based on formaldehyde assimilation into homoserine catalysed by the enzymes HAL and HAT of the synthetic homoserine cycle (He et al., 2020). Formaldehyde is first condensed with pyruvate to generate the intermediate HOB, which is subsequently aminated to homoserine (Figure 4A). In *E. coli*, the HAL reaction is promiscuously catalysed by 2-keto-3-deoxy-L-rhamnonate aldolase (RhmA) (Hernandez et al., 2017). The HAT reaction is catalysed by endogenous aminotransferases (Hernandez et al., 2017; Walther et al., 2018; Zhong et al., 2019). To create a formaldehyde biosensor based on these reactions, a homoserine auxotrophic strain that depends on formaldehyde assimilation via HAL and HAT to relief the auxotrophy needs to be created. The HOB biosensor has an estimated formaldehyde dependency of 0.70 mmol/gCDW.

The deletion of all the required genes together with the endogenous *rhmA* gene (see Figure 4A) led to the creation of the HOB parent strain (HOB_{Parent}). We then expressed *rhmA* with rbsC or rbsA under the control of a constitutive promoter from the genome creating HOB_C and HOB_A. The growth of both strains expressing SoxA from a plasmid was tested with a defined concentration of sarcosine (Figure 4B). As the HOB_A biosensor showed better growth, it was used in all further experiments. We performed a detailed characterization experiment with a sarcosine gradient to examine the sensitivity of the strain (Figure 4C). The strain was able to grow with concentrations as low as 125 μM sarcosine, making it more sensitive than the other two biosensors. As the sensitivity of the HOB biosensor could be further increased by supplementing either methionine or threonine (neither amino acid can be converted to homoserine, thus allowing supplementation without risking a complete relief of the auxotrophies), we tested the addition of either amino acid to the selective medium. An initial experiment suggested that supplementation of methionine does not improve the sensitivity of the strain whereas supplementation of threonine does (Figure S4). Thus, we conducted a formaldehyde sensitivity experiment with threonine supplementation (Figure 4D). Notably, the addition of threonine reduces the formaldehyde dependency of the strain to 0.15 mmol/gCDW (as estimated by FBA). By repeating the gradient experiment with supplementation of 1 mM threonine, the strain was capable of growing with sarcosine concentrations as low as 30 μM, making it by far the most sensitive formaldehyde biosensor.

Comparison of formaldehyde sensitivity reveals the operational range of the biosensors

After characterizing the biosensor strains in detail, we aimed to systematically compare their formaldehyde sensitivity and to determine their operational range. The operational range is the range of formaldehyde concentrations over which the biosensor exhibits a detectable change in the final OD_{600} (Rogers et al., 2016). To this end, we determined the maximum OD_{600} reached by the respective biosensor at a given sarcosine concentration and plotted the data in a sensitivity plot (Figure 5A). When comparing all strains, it becomes clear that the HOB_A biosensor with supplementation of threonine is the most sensitive strain followed by HOB_A without supplementation, $LtaE^*_A$, $LtaE_A$ and the $RuMP_A$ sensor. As the operational ranges of the sensors overlap (especially for HOB_A, $LtaE^*_A$ and $LtaE_A$), we suggest to use the formaldehyde biosensors in the following way: the HOB_A biosensor (with the addition of threonine) should be used for detecting formaldehyde

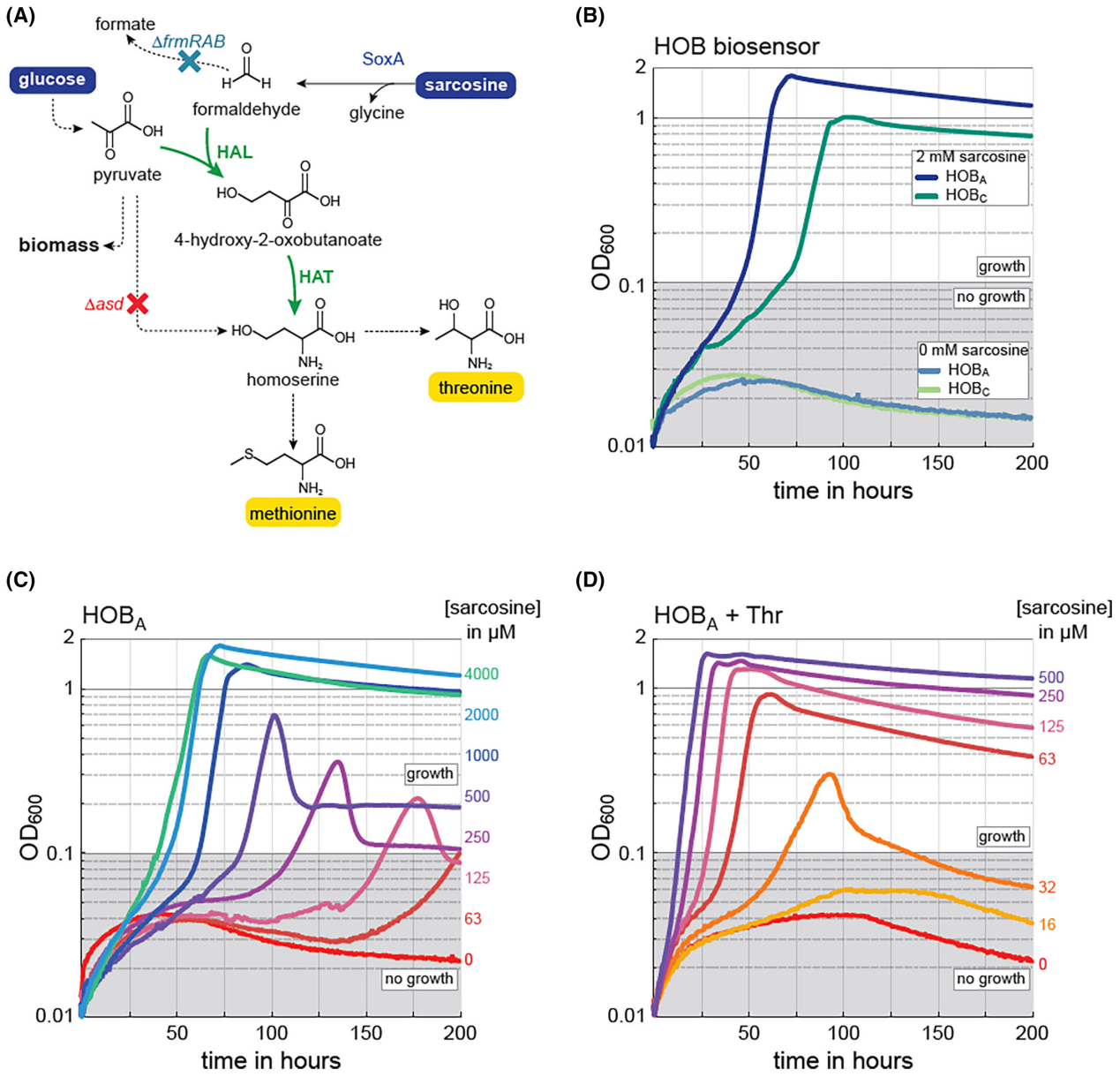

FIGURE 4 The HOB biosensor detects formaldehyde in the low micromolar range. (A) Metabolic scheme of the HOB biosensor. The strain utilizes HAL and HAT activities to convert formaldehyde and pyruvate into homoserine. In the HOB biosensor, the native homoserine biosynthesis pathway is knocked out making it auxotrophic for threonine and methionine. These auxotrophies can be relieved by the assimilation of intracellular formaldehyde via HAL and HAT. To allow formaldehyde assimilation, the HAL gene was expressed from the genome using a strong constitutive promoter and either a medium or strong ribosome binding site (rbsC or rbsA, respectively). SoxA was expressed from a plasmid to allow sarcosine oxidation to formaldehyde. (B) The HOB_C and HOB_A biosensors were cultivated in a minimal medium containing all relevant carbon sources with and without the addition of 2 mM sarcosine. (C) As the HOB_A biosensor was shown to be more sensitive, it was used for detailed characterization of its formaldehyde sensitivity. The strain was cultivated with a gradient of sarcosine concentrations and showed growth correlation in a range from 125 to 2000 µM. (D) When 1 mM threonine was supplemented to reduce the formaldehyde dependency of the strain, the HOB_A biosensor was capable of growing on sarcosine concentrations as low as 32 µM. *Asd*, aspartate semialdehyde dehydrogenase; *frmRAB*, formaldehyde detoxification system; SoxA, sarcosine oxidase; HAL, HOB aldolase; HAT, HOB aminotransferase. Figure elements: Yellow background: Auxotrophy; blue circle: Substrate; red cross: Deletion causing auxotrophy; cyan cross: Non-essential deletion; green arrow: Formaldehyde assimilation flux; dashed arrow: Multi enzymatic reaction.

concentrations between 30 and 200 µM, the $LtaE^*_A$ biosensor for concentrations between 200 µM and 1 mM and the $RuMP_A$ biosensor for concentrations between 1 and 10 mM (Figure 5B). In this combination, the formaldehyde biosensors present an operational range that spans almost three orders of magnitude, allowing for a wide range of applications.

Benchmarking of biotechnologically relevant MDHs in the HOB sensor

After determining the formaldehyde sensitivities of the different biosensors, we aimed to test their applicability for assessing formaldehyde producing enzymes. This could be highly useful for enzyme engineering efforts

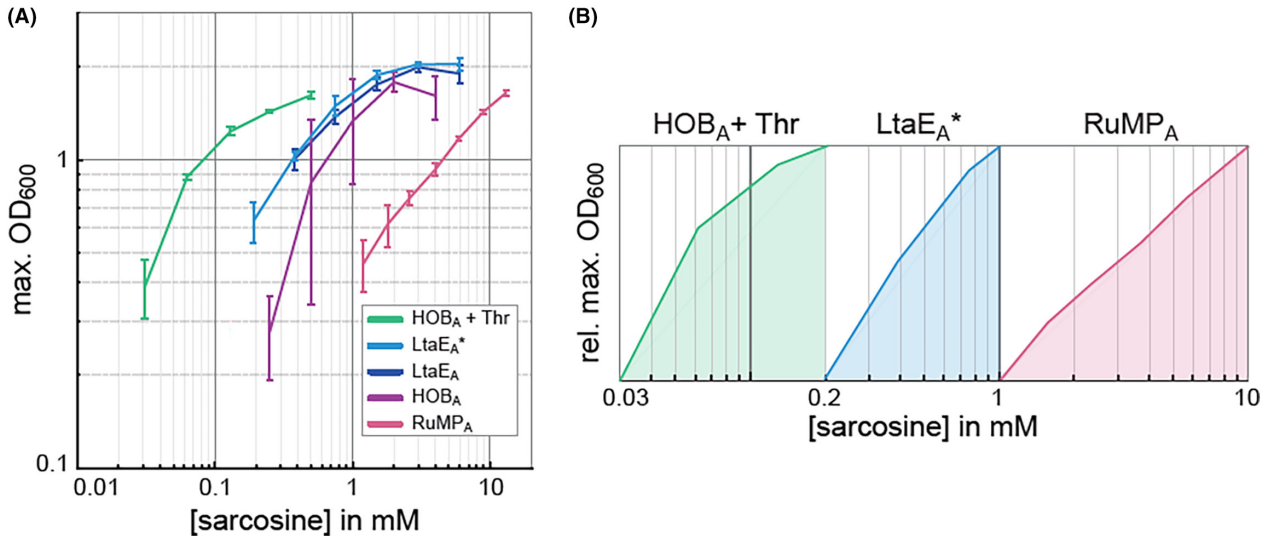

FIGURE 5 Comparison of formaldehyde sensitivities reveals the operational range of the biosensors. (A) To create a sensitivity plot that allows a direct comparison of all formaldehyde biosensors created in this work, the mean maximum OD_{600} was plotted against sarcosine concentrations. (B) Together, the HOB_A biosensor (with the addition of threonine), the $LtaE^*_A$ biosensor, and the $RuMP_A$ biosensor present an operational range from 0.03 to 10 mM, spanning almost 3 orders of magnitude. For each concentration of sarcosine, the average maximum OD_{600} of three independent growth experiments is shown and standard deviations are represented by error bars.

TABLE 1 In vitro characteristics of MDH variants tested in the HOB sensor.

		In vitro data		
MDH	**Source organism**	**K_M [mM]**	**V_{max} [U/mg]**	**Reference**
*Bs*MDH	*Bacillus stearothermophilus*	20	2.1	Whitaker et al. (2017)
*Cn*MDH	*Cupriavidus necator N-1*	22	0.3	Wu et al. (2016)
*Bm*MDH	*Bacillus methanolicus*	432	0.13	Roth et al. (2019)
*Cg*MDH	*Corynebacterium glutamicum*	3	0.7	Kotrbova-Kozak et al. (2007)

or the discovery of natural formaldehyde producing enzymes. As NADH-dependent MDHs (which often pose a bottleneck in synthetic C_1 metabolism studies (Krüsemann et al., 2023)) are probable engineering candidates, we decided to compare the in vivo activity of widely used MDHs (*Bs*MDH, *Cn*MDH, *Bm*MDH and *Cg*MDH) using the HOB_A biosensor. To this end, we transformed the strain with a plasmid encoding the respective MDH (see Table 1 for details about the MDHs) and tested the strain's growth with different methanol concentrations (Figure 6A). While all tested MDHs supported growth of the HOB_A biosensor at methanol concentrations of 80 and 40 mM, only one MDH (*Bs*MDH, which resulted in highest OD_{600} for all tested methanol concentrations) was able to provide sufficient formaldehyde to enable growth of the strain at 10 mM methanol. With 20 mM methanol, the difference between the MDH variants can be compared best (Figure 6B). While *Bs*MDH still enables fast growth to a relatively high OD_{600}, *Cn*MDH and *Cg*MDH enable mediocre growth and *Bm*MDH hardly enables growth of the strain. Looking at the max. OD_{600} and the DT at different concentrations (Figure 6C,D), it becomes clear that the *Bs*MDH has by far the best in vivo activity followed by *Cn*MDH and *Cg*MDH. These results roughly correlate with published in vitro data (Table 1) and in vivo data (Wenk et al., 2020) which show that *Bs*MDH has the highest catalytic activity among all tested variants. Only *Cn*MDH and *Cg*MDH differ from the published in vitro results as they lead to similar growth phenotypes even though *Cg*MDH supposedly has a lower K_M and a higher V_{max} than *Cn*MDH. Overall, these results demonstrate the applicability of the formaldehyde biosensors for testing the in vivo activity of formaldehyde generating enzymes.

DISCUSSION

In the present work, we developed a growth-coupled strategy for the creation of three distinct formaldehyde biosensors. By strategically interrupting central metabolic fluxes through gene deletions, we made the strains dependent on formaldehyde assimilation for cellular growth. Formaldehyde assimilation was enabled through genomic expression of formaldehyde assimilating enzymes and verified by various experiments. Together, these biosensors can detect a wide range of

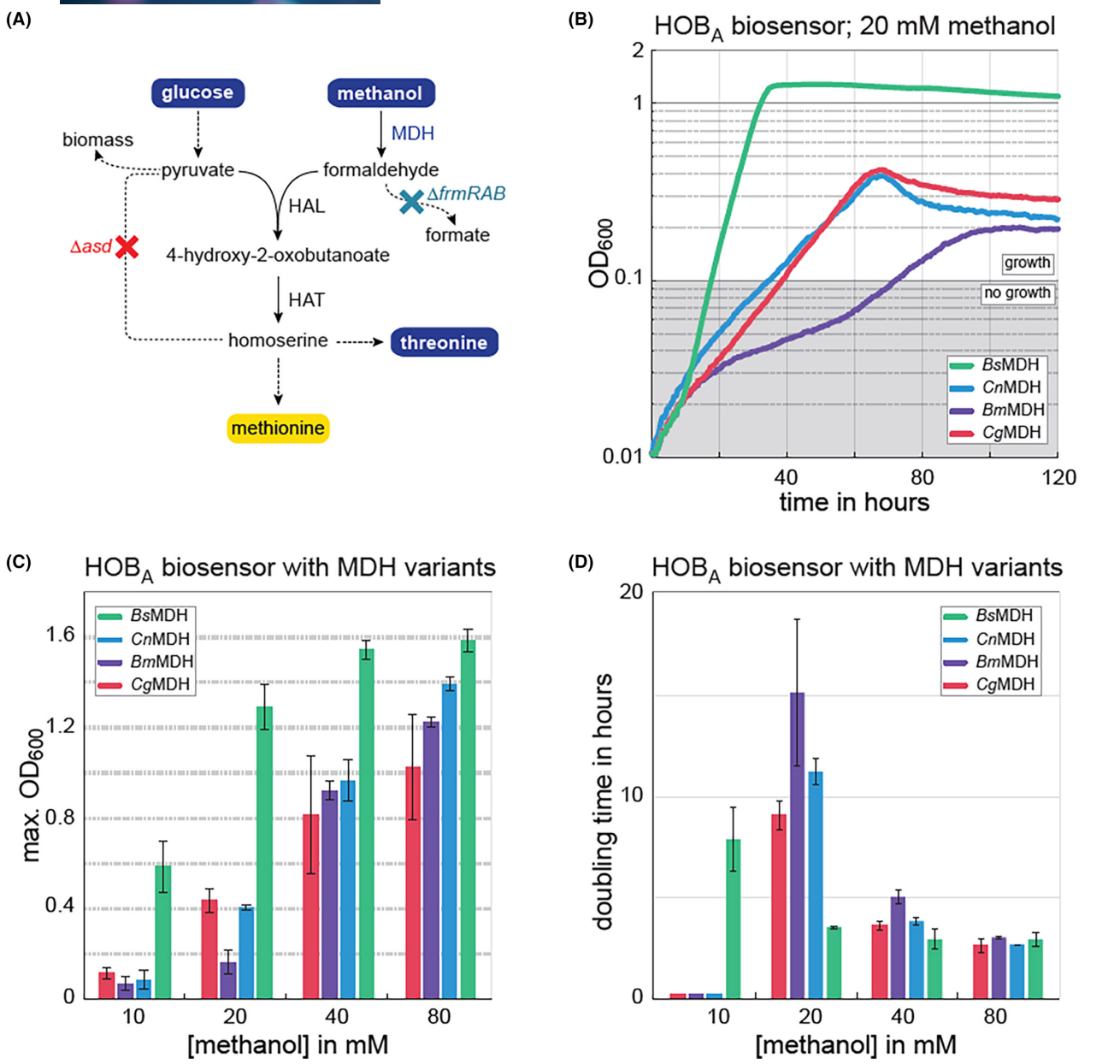

FIGURE 6 Assessment of in vivo activities of different methanol dehydrogenases in the HOB biosensor. (A) MDH expression in the HOB$_A$ biosensor allows methanol oxidation to formaldehyde and its subsequent assimilation into homoserine. Different biotechnologically relevant MDHs were expressed from a plasmid in the HOB$_A$ biosensor. (B–D) The resulting strains were cultivated in minimal media containing all relevant carbon sources and 10 to 80 mM methanol. (B) With 20 mM methanol, the difference between the MDH variants became most obvious. (C) While all MDH variants rescued growth at 80 mM methanol, only *Bs*MDH was capable of rescuing growth at 10 mM methanol. Furthermore, *Bs*MDH resulted in the highest max. OD$_{600}$ with all tested methanol concentrations. (D) The doubling time (DT) of the different strains increased with lower methanol concentration. At 20 mM methanol, the difference in DT is most pronounced. With 10 mM methanol, only the DT for *Bs*MDH is shown as it is the only enzyme that enabled growth at this concentration. *Asd*, aspartate semialdehyde dehydrogenase; *frmRAB*, formaldehyde detoxification system; *Bs*MDH, *Bacillus stearothermophilus* MDH; *Bm*MDH, engineered *Bacillus methanolicus* MDH; *Cg*MDH, *Corynebacterium glutamicum* MDH; *Cn*MDH, engineered *Cupriavidus necator* N-1 MDH; HAL, HOB aldolase; HAT, HOB aminotransferase. Figure elements: Yellow circle, auxotrophy; blue circle, substrate; red cross, deletion causing auxotrophy; cyan cross, non-essential deletion; dashed arrow, multi enzymatic reaction.

intracellular formaldehyde concentrations spanning almost three orders of magnitude.

In the design phase of this study, we assessed the formaldehyde dependency of the biosensors via FBA in order to create three strains with different sensitivities. Our results suggested that the RuMP biosensor would be the most sensitive followed by the LtaE and the HOB biosensor. Since the FBA modelling did not consider important cellular factors like enzyme kinetics and co-factor availability, it is of little surprise, that the experimental validation of the strains resulted in a different picture than the computational prediction:

While the engineered strains differ in their respective formaldehyde sensitivity, the characterization experiments resulted in the HOB_A biosensor being the most sensitive followed by $LtaE_A$ and $RuMP_A$. This shows clearly that FBA is a good tool for a priori estimations but cannot replace experimental validations.

In a previous study, a highly sensitive transcription-based formaldehyde biosensor that leads to GFP expression upon detection of intracellular formaldehyde was engineered by Woolston et al. (Woolston et al., 2018). This sensor detects formaldehyde with an operational range of ~1 to ~250 μM within 1.5 h. While this sensor leads to a faster signal than the growth biosensors, it cannot be used to detect higher formaldehyde concentrations and cannot assess whether the formaldehyde-producing enzyme carries sufficient flux to support cell growth. Furthermore, it requires a more advanced technical setup and could be problematic for multiplexed experiments due to signal interference. Also, long-term experiments might be difficult due to the plasmidic nature of the sensor. Thus, the growth biosensors presented in this work, which together present an operational range of ~30 μM to ~13 mM, ideally complement the work of Woolston et al. and increase the operational range of available cell-based formaldehyde biosensors by several orders of magnitude. Compared to the GFP-based sensor, our growth biosensors are fully genomic allowing transformation with a plasmid library without compatibility issues. Furthermore, they produce an easy-to-detect signal: cell growth, allowing simple and cheap detection methods. Due to the stringent design, the sensor strains are metabolically robust allowing their use in long-term ALE experiments.

Compared to other methods for formaldehyde detection like the widely used NASH assay or electrochemical biosensors, the cellular formaldehyde sensors present several advantages. On one hand, they allow direct detection and approximate quantification of intracellular formaldehyde (other sensors usually detect extracellular formaldehyde). On the other hand, they allow to work in a living system which has several advantages by itself. The biosensors are self-replicating and do not need any tedious preparation. They can be applied for live monitoring of formaldehyde concentrations, where an increase in formaldehyde would lead to an increase of the max. OD_{600}. As such, they are ideally suited for in vivo enzyme engineering. Furthermore, they enable multiplexing especially with respect to testing large enzyme libraries.

Due to the wide operational range, the biosensors could be used for applications ranging from enzyme discovery to enzyme engineering. As showcased by the comparison of in vivo catalytic efficiencies of biotechnologically relevant MDHs, the sensor strains can be easily employed as plug-and-play devices for screening libraries of formaldehyde-producing enzymes. Here, a highly sensitive strain like the HOB_A biosensor could be used to identify activities in an unknown library (e.g., a metagenomic library). In contrast, the less sensitive strains could be used for comparing efficiencies of engineered enzymes that are already known to have basal activities. Ultimately, the $RuMP_A$ biosensor could be used for screening very efficient enzymes producing formaldehyde at high rates. To this end, the formaldehyde dependency of the RuMP biosensor could be further increased by excluding succinate from the growth medium (see Figure 2A). This would require the assimilation of formaldehyde (and xylose) for the generation of all biomass and thus require a very high flux through the formaldehyde-producing enzyme (see (He et al., 2018) for more details).

Taken together, the formaldehyde biosensors created in this work, present an ideal platform for enzyme discovery and enzyme engineering studies that aim to find or improve formaldehyde producing enzymes.

AUTHOR CONTRIBUTIONS

Karin Schann: Conceptualization; formal analysis; investigation; methodology; visualization; writing – original draft; writing – review and editing. **Jenny Bakker:** Formal analysis; investigation; methodology; validation; writing – original draft. **Maximilian Boinot:** Formal analysis; investigation; methodology; validation; writing – original draft. **Pauline Kuschel:** Investigation; validation. **Hai He:** Investigation; methodology; software; validation; writing – original draft. **Maren Nattermann:** Formal analysis; investigation; methodology; validation; visualization; writing – original draft. **Nicole Paczia:** Methodology; formal analysis; validation. **Tobias Erb:** Funding acquisition; project administration; resources; supervision. **Arren Bar-Even:** Conceptualization; funding acquisition; project administration; resources; supervision. **Sebastian Wenk:** Conceptualization; formal analysis; methodology; project administration; supervision; visualization; writing – original draft; writing – review and editing.

ACKNOWLEDGEMENTS

This work was supported by the German Ministry of Education and Research Grant 031B0850B (MetAFor) and the Max Planck Society. The authors are grateful to Arren Bar-Even who initiated the project and was an inspiring mentor to all of us. The authors thank Peter Claus for performing the HPLC-MS measurements and Enrico Orsi for critical reading of the manuscript and helpful suggestions.

CONFLICT OF INTEREST STATEMENT

The authors declare no competing interest.

DATA AVAILABILITY STATEMENT

Additional information on the experimental setup as well as detailed results are available from the corresponding

author upon request. Any strains and plasmids generated during this study are available upon completing a Materials Transfer Agreement.

ORCID

Karin Schann https://orcid.org/0000-0003-1548-7643
Jenny Bakker https://orcid.org/0009-0001-0503-8708
Maximilian Boinot https://orcid.org/0009-0004-2977-2175
Hai He https://orcid.org/0000-0003-1223-2813
Maren Nattermann https://orcid.org/0000-0003-0649-8447
Nicole Paczia https://orcid.org/0000-0003-3859-8186
Tobias Erb https://orcid.org/0000-0003-3685-0894
Arren Bar-Even https://orcid.org/0000-0002-1039-4328
Sebastian Wenk https://orcid.org/0000-0001-9404-3535

REFERENCES

Antoniewicz, M.R. (2019) Synthetic methylotrophy: strategies to assimilate methanol for growth and chemicals production. *Current Opinion in Biotechnology*, 59, 165–174.

Aslan, S., Noor, E., Benito Vaquerizo, S., Lindner, S.N. & Bar-Even, A. (2020) Design and engineering of *E. Coli* metabolic sensor strains with a wide sensitivity range for glycerate. *Metabolic Engineering*, 57, 96–109.

Baba, T., Ara, T., Hasegawa, M., Takai, Y., Okumura, Y., Baba, M. et al. (2006) Construction of *Escherichia coli K-12* in-frame, single-gene knockout mutants: the Keio collection. *Molecular Systems Biology*, 2, 2006.0008.

Bar-Even, A. (2016) Formate assimilation: the metabolic architecture of natural and synthetic pathways. *Biochemistry*, 55, 3851–3863.

Barrick, J.E., Colburn, G., Deatherage, D.E., Traverse, C.C., Strand, M.D., Borges, J.J. et al. (2014) Identifying structural variation in haploid microbial genomes from short-read resequencing data using breseq. *BMC Genomics*, 15, 1–17.

Bowker, M. (2019) Methanol synthesis from CO_2 hydrogenation. *ChemCatChem*, 11, 4238–4246.

Chen, F.Y.H., Jung, H.W., Tsuei, C.Y. & Liao, J.C. (2020) Converting *Escherichia coli* to a synthetic Methylotroph growing solely on methanol. *Cell*, 182, 933–946.e14.

Claassens, N.J., Bordanaba-Florit, G., Cotton, C.A.R., De Maria, A., Finger-Bou, M., Friedeheim, L. et al. (2020) Replacing the Calvin cycle with the reductive glycine pathway in *Cupriavidus necator*. *Metabolic Engineering*, 62, 30–41.

Claassens, N.J., Cotton, C.A.R., Kopljar, D. & Bar-Even, A. (2019) Making quantitative sense of electromicrobial production. *Nature Catalysis*, 2, 437–447.

Contestabile, R., Paiardini, A., Pascarella, S., Di Salvo, M.L., D'Aguanno, S. & Bossa, F. (2001) L-threonine aldolase, serine hydroxymethyltransferase and fungal alanine racemase: a subgroup of strictly related enzymes specialized for different functions. *European Journal of Biochemistry*, 268, 6508–6525.

Dietrich, J.A., McKee, A.E. & Keasling, J.D. (2010) High-throughput metabolic engineering: advances in small-molecule screening and selection. *Annual Review of Biochemistry*, 79, 563–590.

Ebrahim, A., Lerman, J.A., Palsson, B.O. & Hyduke, D.R. (2013) COBRApy: COnstraints-based reconstruction and analysis for python. *BMC Systems Biology*, 7, 1–6.

Espinosa, M.I., Gonzalez-Garcia, R.A., Valgepea, K., Plan, M.R., Scott, C., Pretorius, I.S. et al. (2020) Adaptive laboratory evolution of native methanol assimilation in *Saccharomyces cerevisiae*. *Nature Communications*, 11, 5564.

García, J.L. & Galán, B. (2022) Integrating greenhouse gas capture and C1 biotechnology: a key challenge for circular economy. *Microbial Biotechnology*, 15, 228–239.

Gupta, N., Renugopalakrishnan, V., Liepmann, D., Paulmurugan, R. & Malhotra, B.D. (2019) Cell-based biosensors: recent trends, challenges and future perspectives. *Biosensors & Bioelectronics*, 141, 111435.

He, H., Edlich-Muth, C., Lindner, S.N. & Bar-Even, A. (2018) Ribulose monophosphate shunt provides nearly all biomass and energy required for growth of *E. Coli*. *ACS Synthetic Biology*, 7, 1601–1611.

He, H., Höper, R., Dodenhöft, M., Marlière, P. & Bar-Even, A. (2020) An optimized methanol assimilation pathway relying on promiscuous formaldehyde-condensing aldolases in *E. Coli*. *Metabolic Engineering*, 60, 1–13.

Hernandez, K., Bujons, J., Joglar, J., Charnock, S.J., Domínguez De María, P., Fessner, W.D. et al. (2017) Combining aldolases and transaminases for the synthesis of 2-Amino-4-hydroxybutanoic acid. *ACS Catalysis*, 7, 1707–1711.

Herschkovitz, Y., Eshkenazi, I., Campbell, C.E. & Rishpon, J. (2000) An electrochemical biosensor for formaldehyde. *Journal of Electroanalytical Chemistry*, 491, 182–187.

Hu, G., Guo, L., Gao, C., Song, W., Liu, L. & Chen, X. (2022) Synergistic metabolism of glucose and Formate increases the yield of short-chain organic acids in *Escherichia coli*. *ACS Synthetic Biology*, 11, 135–143.

Ikeda, H. & Tomizawa, J.I. (1965) Transducing fragments in generalized transduction by phage P1: III. Studies with small phage particles. *Journal of Molecular Biology*, 14, 120–129.

Jensen, S.I., Lennen, R.M., Herrgård, M.J. & Nielsen, A.T. (2015) Seven gene deletions in seven days: Fast generation of *Escherichia coli* strains tolerant to acetate and osmotic stress. *Scientific Reports*, 5, 1–10.

Keller, P., Reiter, M.A., Kiefer, P., Gassler, T., Hemmerle, L., Christen, P. et al. (2022) Generation of an *Escherichia coli* strain growing on methanol via the ribulose monophosphate cycle. *Nature Communications*, 13, 5243.

Kim, S., Lindner, S.N., Aslan, S., Yishai, O., Wenk, S., Schann, K. et al. (2020) Growth of *E. Coli* on formate and methanol via the reductive glycine pathway. *Nature Chemical Biology*, 16, 538–545.

Kotrbova-Kozak, A., Kotrba, P., Inui, M., Sajdok, J. & Yukawa, H. (2007) Transcriptionally regulated adhA gene encodes alcohol dehydrogenase required for ethanol and n-propanol utilization in *Corynebacterium glutamicum* R. *Applied Microbiology and Biotechnology*, 76, 1347–1356.

Krüsemann, J.L., Rainaldi, V., Cotton, C.A., Claassens, N.J. & Lindner, S.N. (2023) The cofactor challenge in synthetic methylotrophy: bioengineering and industrial applications. *Current Opinion in Biotechnology*, 82, 102953.

Le, T.K., Lee, Y.J., Han, G.H. & Yeom, S.J. (2021) Methanol dehydrogenases as a key biocatalysts for synthetic Methylotrophy. *Frontiers in Bioengineering and Biotechnology*, 9, 1–11.

Ling, Y.P. & Heng, L.Y. (2010) A potentiometric formaldehyde biosensor based on immobilization of alcohol oxidase on acryloxysuccinimide-modified acrylic microspheres. *Sensors (Switzerland)*, 10, 9963–9981.

Marzuki, N.I., Bakar, F.A., Salleh, A.B., Heng, L.Y., Yusof, N.A. & Siddiquee, S. (2012) Development of electrochemical biosensor for formaldehyde determination based on immobilized enzyme. *International Journal of Electrochemical Science*, 7, 6070–6081.

Monk, J.M., Lloyd, C.J., Brunk, E., Mih, N., Sastry, A., King, Z. et al. (2017) *i*ML1515, a knowledgebase that computes *Escherichia coli* traits. *Nature Biotechnology*, 35, 904–908.

Nash, T. (1953) The colorimetric estimation of formaldehyde by means of the Hantzsch reaction. *The Biochemical Journal*, 55, 416–421.

Nattermann, M., Wenk, S., Pfister, P., He, H., Lee, S.H., Szymanski, W. et al. (2023) Engineering a new-to-nature cascade for phosphate-dependent formate to formaldehyde conversion *in vitro* and *in vivo*. *Nature Communications*, 14, 2682.

Nishiya, Y., Yamamoto, M., Takemoto, J., Kano, S. & Nakano, S. (2016) Monomeric sarcosine oxidase exhibiting high substrate affinity and thermostability. *International Journal of Analytical Bio-Science*, 4, 55–62.

Orsi, E., Claassens, N.J., Nikel, P.I. & Lindner, S.N. (2021) Growth-coupled selection of synthetic modules to accelerate cell factory development. *Nature Communications*, 12, 1–5.

Rogers, J.K., Taylor, N.D. & Church, G.M. (2016) Biosensor-based engineering of biosynthetic pathways. *Current Opinion in Biotechnology*, 42, 84–91.

Roth, T.B., Woolston, B.M., Stephanopoulos, G. & Liu, D.R. (2019) Phage-assisted evolution of *bacillus methanolicus* methanol dehydrogenase 2. *ACS Synthetic Biology*, 8, 796–806.

Schada Von Borzyskowski, L., Remus-Emsermann, M., Weishaupt, R., Vorholt, J.A. & Erb, T.J. (2015) A set of versatile brick vectors and promoters for the assembly, expression, and integration of synthetic operons in *methylobacterium extorquens am1* and other alphaproteobacteria. *ACS Synthetic Biology*, 4, 430–443.

Siegel, J.B., Smith, A.L., Poust, S., Wargacki, A.J., Bar-Even, A., Louw, C. et al. (2015) Computational protein design enables a novel one-carbon assimilation pathway. *Proceedings of the National Academy of Sciences of the United States of America*, 112, 3704–3709.

Walther, T., Calvayrac, F., Malbert, Y., Alkim, C., Dressaire, C., Cordier, H. et al. (2018) Construction of a synthetic metabolic pathway for the production of 2,4-dihydroxybutyric acid from homoserine. *Metabolic Engineering*, 45, 237–245.

Wang, J., Anderson, K., Yang, E., He, L. & Lidstrom, M.E. (2021) Enzyme engineering and *in vivo* testing of a formate reduction pathway. *Synthetic Biology*, 6, ysab020.

Wenk, S., Schann, K., He, H., Rainaldi, V., Kim, S., Lindner, S.N. et al. (2020) An "energy-auxotroph" *Escherichia coli* provides an in vivo platform for assessing NADH regeneration systems. *Biotechnology and Bioengineering*, 117, 3422–3434.

Wenk, S., Yishai, O., Lindner, S.N. & Bar-Even, A. (2018) An engineering approach for rewiring microbial metabolism. *Methods in Enzymology*, 608, 329–367.

Whitaker, W.B., Jones, J.A., Bennett, R.K., Gonzalez, J.E., Vernacchio, V.R., Collins, S.M. et al. (2017) Engineering the biological conversion of methanol to specialty chemicals in *Escherichia coli*. *Metabolic Engineering*, 39, 49–59.

Whitaker, W.B., Sandoval, N.R., Bennett, R.K., Fast, A.G. & Papoutsakis, E.T. (2015) Synthetic methylotrophy: engineering the production of biofuels and chemicals based on the biology of aerobic methanol utilization. *Current Opinion in Biotechnology*, 33, 165–175.

Woolston, B.M., Roth, T., Kohale, I., Liu, D.R. & Stephanopoulos, G. (2018) Development of a formaldehyde biosensor with application to synthetic methylotrophy. *Biotechnology and Bioengineering*, 115, 206–215.

Wu, T.Y., Chen, C.T., Liu, J.T.J., Bogorad, I.W., Damoiseaux, R. & Liao, J.C. (2016) Characterization and evolution of an activator-independent methanol dehydrogenase from *Cupriavidus necator N-1*. *Applied Microbiology and Biotechnology*, 100, 4969–4983.

Yishai, O., Lindner, S.N., Gonzalez de la Cruz, J., Tenenboim, H. & Bar-Even, A. (2016) The formate bio-economy. *Current Opinion in Chemical Biology*, 35, 1–9.

Zelcbuch, L., Antonovsky, N., Bar-Even, A., Levin-Karp, A., Barenholz, U., Dayagi, M. et al. (2013) Spanning high-dimensional expression space using ribosome-binding site combinatorics. *Nucleic Acids Research*, 41, e98.

Zhang, W., Zhang, T., Wu, S., Wu, M., Xin, F., Dong, W. et al. (2017) Guidance for engineering of synthetic methylotrophy based on methanol metabolism in methylotrophy. *RSC Advances*, 7, 4083–4091.

Zhong, W., Zhang, Y., Wu, W., Liu, D. & Chen, Z. (2019) Metabolic engineering of a Homoserine-derived non-natural pathway for the de novo production of 1,3-Propanediol from glucose. *ACS Synthetic Biology*, 8, 587–595.

SUPPORTING INFORMATION

Additional supporting information can be found online in the Supporting Information section at the end of this article.

How to cite this article: Schann, K., Bakker, J., Boinot, M., Kuschel, P., He, H., Nattermann, M. et al. (2024) Design, construction and optimization of formaldehyde growth biosensors with broad application in biotechnology. *Microbial Biotechnology*, 17, e14527. Available from: https://doi.org/10.1111/1751-7915.14527